Journal Name

ARTICLE

NMR analysis of the binding mode of two fungal endo β-1,4-mannanases from GH5 and GH26 families

Roberta Marchetti, [a]* Jean-Guy Berrin, [b] Marie Couturier, [b] Shah Ali Ul Qader, [a,c] Antonio Molinaro[a] and Alba Silipo[a]*

The enzymatic digestion of the main components of lignocellulosic biomass, including plant cell wall mannans, constitutes a fundamental step in the renewable biofuel production, with great potential benefit in the industrial field. Despite several reports of X-ray structures of glycoside hydrolases, how polysaccharides are specifically recognized and accommodated in the enzymes binding site still remains a pivotal matter of research. Within this frame, NMR spectroscopic techniques provide key binding information, complementing and/or enhancing the structural view by X-ray crystallography. Here we present deep insights into the binding mode of two endo-β-1,4 mannanases from the coprophilous ascomycete *Podospora anserina*, *Pa*Man26A and *Pa*Man5A, involved in the hydrolysis of plant cell wall mannans and heteromannans. The investigation at a molecular level of the interaction between the wild-type enzymes and inactive mutants with *manno*-oligosaccharides, revealed a different mode of action among the two glycoside hydrolases most likely due to the presence of the additional and peculiar -4 subsite in the *Pa*Man26A binding pocket.

Introduction

Lignocellulose is one of the main constituents of plants, providing rigidity and structure to the cell wall, and represents the main source of renewable organic material. It primarily consists of lignin, cellulose, pectins and hemicelluloses, with proportion varying among plant species and tissues.[1] In turn, hemicelluloses include structural polysaccharides among which mannans are one of the most important members, mainly found in softwood (galactoglucomannan) but present in smaller amount also in hardwood (glucomannan).[2] In nature, different forms of mannans are observed; they comprise homogeneous linear polymers composed by β-1,4-linked mannose residues, referred to as mannan, or heterogeneous polysaccharides formed by a combination of different building blocks of glucose and mannose residues. In addition, each type of mannan-based polymer can be decorated occasionally with side chains of α-1,6-linked galactose

residues. Beyond their structural functions, mannans serve as seed storage and are involved in plant cell differentiation as key signaling molecules.[3] Due to the possibility to use mannans in biorefinery process as an alternative to the petroleum-based materials, there is an increasing attention on the study of their value-added applications and hydrolysis.

The bioconversion of renewable biomass is initiated primarily by microorganisms, such as bacteria and fungi,[4] which are characterized by complex lignocellulolytic enzymatic machineries, including a great variety of glycoside hydrolases (GHs). The term glycoside hydrolases refers to a widespread group of enzymes, ubiquitous in nature, with the capability to catalyze the hydrolysis of O-, N- and S- glycosidic bonds. Since, in the years, a plethora of amino acid sequences have been identified as GHs, the classification in families, based on several parameters, including mechanism of action and structural fold, nowadays results in 133 different families.[5] This list is constantly growing and continuously updated at the Carbohydrate-Active Enzymes (CAZy) server (http://www.cazy.org). As a consequence of GHs substrate diversity, it is not surprising that glycosidases play a key role in a broad spectrum of biological processes, including glycoprotein maturation, cellular homeostasis and primary metabolism.[6] On the other hand, their ability to degrade polysaccharides found as storage and structural polymers in plant cell walls have drawn a lot of attention on a variety of GHs applications in industrial and biotechnological fields.[7] In the last years, many efforts were directed toward the optimization of the GHs role in the emerging field of renewable energies.[8] The enzymatic digestion of lignocellulosic materials from abundant and underutilized resources, such as crops and grasses, indeed, constitutes a

[a.] Dr. R. Marchetti, Prof. S. A. Ul Qader, Prof. A. Molinaro, Prof. A.Silipo
Department of Chemical Sciences,
Università di Napoli Federico II, Complesso Universitario Monte S. Angelo,
Via Cintia 4, I-80126, Naples, Italy
E-mail: silipo@unina.it
[b.] Dr. J-G Berrin, Dr. M. Couturier
INRA
UMR1163 BBF
13009 Marseille, France
[c.] Prof. S. A. Ul Qader
The Karachi Institute of Biotechnology and Genetic Engineering (KIBGE)
University of Karachi
Karachi 75270, Pakistan

convenient and sustainable method for the production of second-generation bioethanol.

Among the variety of hydrolytic enzymes belonging to bacterial/ fungal degrading systems and involved in the saccharification of lignocellulosic biomass, β-mannanases are responsible for the cleavage of mannose containing glycoconjugates and polysaccharides. This class of GHs is of a great value in biorefinery process, since, as mentioned above, one of the main hemicellulose component, especially in softwoods, is the β-1,4 mannan.

Although X-ray studies have been used to solve the three dimensional structures of a range of bacterial and fungal β-mannanases,[9,10] refining the knowledge on the structure and function of these plant cell wall degrading enzymes represents a pivotal step to enhance their application as biocatalyst in both biological and industrial field.

Here, we have focused our attention on the glycoside hydrolase families GH26 and GH5, which are crucial in the digestion of plant derived mannans. In detail, we have analyzed two enzymes from the filamentous, ascomycete fungi *Podospora anserina*, belonging respectively to fungal GH26 and GH5 endo-β-1,4 mannanases (herein *Pa*Man26A and *Pa*Man5A). They share some structural features typical for the GH-A clan members, including the (β/α)$_8$-barrel fold, with relatively conserved amino acids, e.g. Glu residues, located at the active site, which function as acid/base and nucleophile. Furthermore, both enzyme families cleave the internal linkages of mannans backbone through a retaining double displacement mechanism.[11] However, the number of substrate-binding subsites necessary to perform an efficient hydrolysis, as well as the interaction within the enzyme-substrate complex, may vary. Recently, it has been shown a different mode of action for the two families of mannanases, GH26 and GH5, which induce the release of different mannan hydrolysis products.[12] This suggested the involvement of different protein subsites in the recognition and interaction with *manno*-oligosaccharides.

In order to improve the knowledge on the *P. anserina* enzymatic machinery involved in the degradation of lignocellulosic biomass, supporting and extending previous analyses,[12] we have investigated the binding mode of the two enzymes, *Pa*Man26A and *Pa*Man5A, in the interaction with several *manno*-oligosaccharides. Specifically, we used Saturation Transfer Difference NMR to gain deep insight into the interacting epitope of *manno*-oligosaccharides of different length for both *Pa*Man26A and *Pa*Man5A. The STD NMR method, indeed, represents a powerful tool not only to discriminate between binders and non-binders, but also to define the ligand regions in intimate contact with the receptor in the case of intermolecular interaction.[13] Thus, STD NMR analysis allowed us to characterize at atomic resolution the binding mode of the two enzymes; in parallel, tr-NOESY experiments have been carried out with the aim to investigate the conformational behavior of mannan substrates.[13,14]

Our results furnished a firm support to previous data, extending the existing view by X-ray and underlying the involvement of different protein subsites in mannans recognition among the two enzyme families.

Results and discussion

Binding epitope of the hydrolysis products to wild-type *Pa*Man26A and *Pa*Man5A.

As a first step toward the comprehension of the binding mode of the two glycoside hydrolases *Pa*Man26A and *Pa*Man5A in the interaction with *manno*-oligosaccharides, we investigated different hydrolysis products in the presence of each enzyme. Saturation Transfer Difference (STD) NMR method was used to unravel the ligand moieties involved in the interaction with the proteins and allowed to map their interacting epitope.[14]

Firstly, we have analyzed the binding of *Pa*Man26A and *Pa*Man5A with D-mannose, one of the typical products derived from the enzymatic hydrolysis of *manno*-oligosaccharides. Upon the addition of the D-mannose, no STD signals were observed neither to *Pa*Man26A nor to *Pa*Man5A (data not shown), indicating that none of the two proteins possessed the ability to bind the free reducing mannose.

In addition, we studied the complex of both enzymes with an other recurring mannan hydrolysis product, the β-1,4-mannotriose, **M3** (see supporting information, Table S1 for NMR assignment). From a qualitative analysis of the two STD NMR spectra, performed under the same experimental conditions, it was clearly inferred that the two enzymes exhibited a different mode of binding (Figure 1, see also supporting information, table S2). The fingerprint of the spectra and the relative intensities of STD signals, indeed, gave a first evidence of a different fashion of substrate accommodation in the protein binding sites.

Although the same protein and ligand concentrations were used for both the analyses, the signal to noise ratio was lower for the interaction of the mannotriose **M3** with *Pa*Man5A respect to that of *Pa*Man26A. It may suggest a lower affinity of the glycosidase *Pa*Man5A for this product. Furthermore, due to the overlapping between some ligand resonances, the quantitative analysis of the STD effects were hindered; however, a qualitative comparison of the STD intensities suggested that the interaction of **M3** with each enzyme preferentially engaged different ligand protons. In both cases, the presence of STD signals ascribable to the three mannose residues indicated that the whole saccharide moiety was accommodated in the binding pocket (Figure 1). However, in the case of *Pa*Man26A interaction with **M3**, the central mannose residue **B**, and especially the proton at position 2, received the largest amount of magnetization, thereby indicating its strong involvement to the binding. In parallel, STD enhancements belonging to the terminal mannose **C** were observed and almost all of them exhibited a level of saturation above 50%. Further information on the ligand binding epitope could be gained by the analysis of the shape of STD signals. For instance, at 3.38 ppm resonated either H4 of terminal residue **C** and H5 of the internal mannose **B**; nevertheless, the presence of a triplet resonating at 3.38 ppm in the STD spectrum allowed to identify it as H4 of residue **C**, suggesting its contribution to the interaction (Figure 1 b-c).

On the contrary, by analyzing STD signals of the **M3** ligand when bound to *Pa*Man5A, the highest transfer of magnetization was observed for the proton at position 2 of the terminal mannose **C**; furthermore, also H6 significantly contributed to the interaction with the protein while other protons within such residue, i.e. H3, H4 and H5, showed a decreased STD intensity (Figure 1 d-e).

Journal Name   ARTICLE
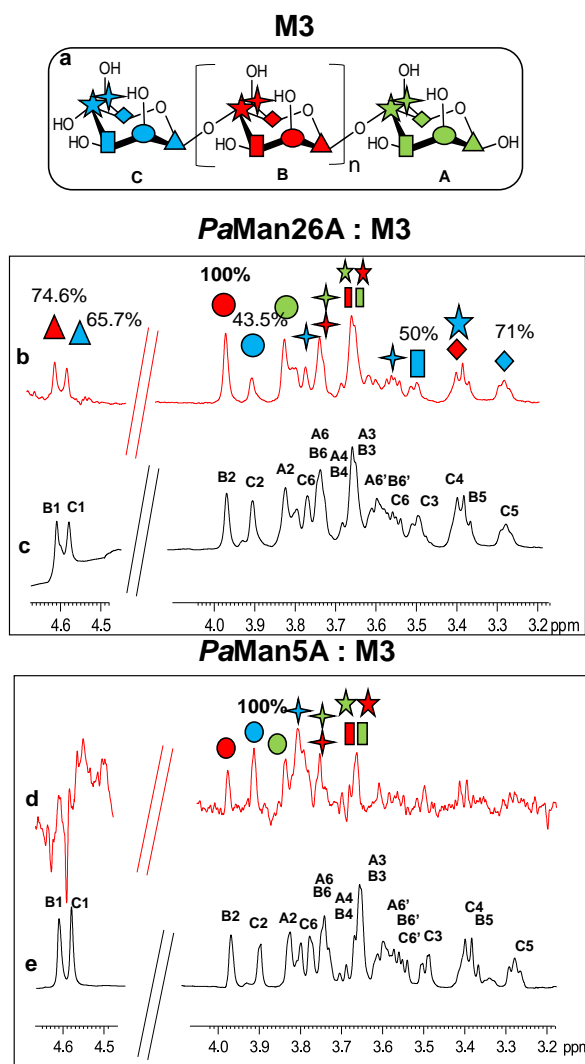
Figure 1. Comparison between the binding of mannotriose, **M3**, to the glycoside hydrolase Pa*Man*26A and Pa*Man*5A.a) Chemical structure of the ligands; n=1 in the case of **M3**; n=3 in the case of **M5**; n=4 in the case of **M6**. Different colored symbols were used to distinguish the different protons on the different sugar residue. b) STD NMR spectrum on the mixture **Pa*Man*26A: M3** 1:50. c) ^{1}H NMR spectrum of the product **M3** in the presence of the enzyme. d) STD NMR spectrum on the mixture **Pa*Man*5A: M3** 1:50. e) ^{1}H NMR spectrum of the product **M3** in the presence of the enzyme. The experiments were carried out at 280K, with a saturation time of 2 sec; the on resonance was set to 0.4ppm. The numbers on the STD spectrum show the normalized levels of saturation (%) received by each ligand proton upon binding with the enzyme.

These outcomes indicated that the two glycoside hydrolases do not share a common mode of binding for *manno*-oligosaccharides. Although both enzymes accommodated the whole oligosaccharide, NMR results suggested the involvement of different protein subsites, in agreement with the previous reported data. [12]

The STD NMR results were then complemented with tr-NOESY analysis in order to investigate the bioactive conformation of the ligand.

In detail, NOESY experiments with different mixing times were performed on the ligand alone in solution and in the presence of each enzyme by using a protein: ligand ratio of 1:20. Negative NOE contacts were observed for the ligand **M3** in both the free and bound state. The overlapping between several signals impaired a
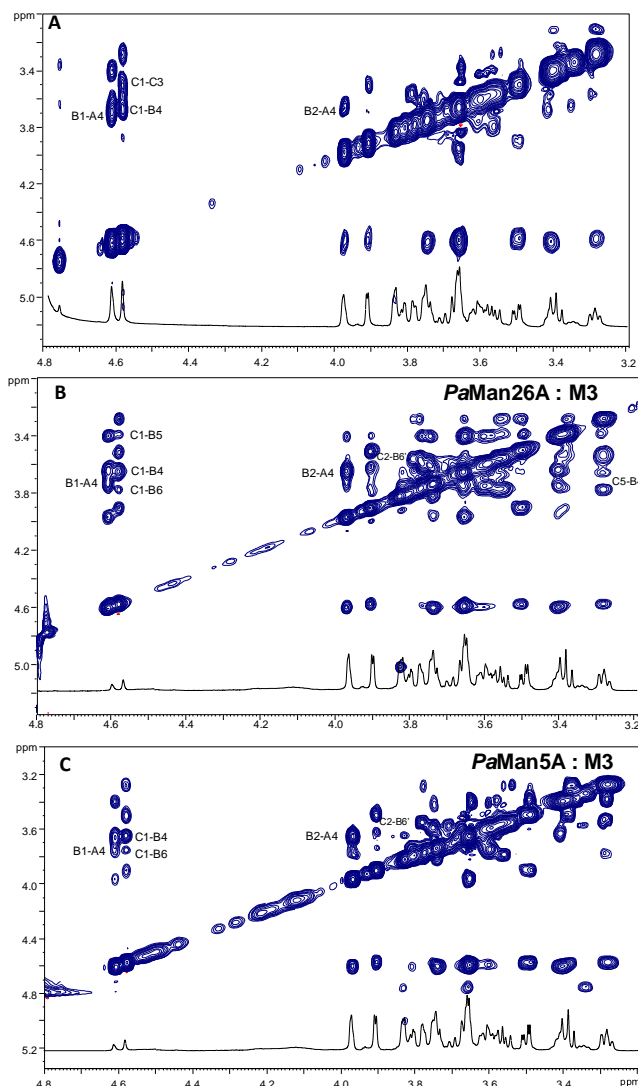
Figure 2. Binding of **M3** to *Pa*Man5A and *Pa*Man26A monitored by transferred NOESY. A section of 2D NOESY experiment carried out on the ligand **M3** in the free state (A) and in the presence of *Pa*Man26A (B) and *Pa*Man5A (C) with a mixing time of 400 ms and a protein ligand ratio 1:20.

detailed study of all important cross peaks; however, a more qualitative evaluation of *inter*-residual NOE signals (Figure 2-3) permitted to deduce that in both free and bound states there was an equilibrium between the two main predicted energetic minima for the β-1,4 linkage (Table 1).

Nevertheless, slight changes in the cross-peaks intensities and in some key *inter*-proton distances were detected in the bound states; indeed, some intermolecular NOE contacts, such as the cross peak C1-B6, were present in tr-NOESY spectra of both systems *Pa*Man26A: **M3** and *Pa*Man5A:**M3**, whereas they were not detected in the NOESY spectrum of the ligand alone. Although thin differences in the cross-peaks intensities between the two bound states were observed (Table 1), the overall results detected a slight preference of **M3** ligand for the minimum characterized from positive values of glycosidic dihedral angles, upon binding to each

Journal Name

ARTICLE

Table 1 Experimental and calculated intermolecular distances for the ligand **M3**.
Nd: not detected. No NOE signal was observed. **Nc**: not calculated. NOE signal was observed but the overlapping unpaired the integration.

	Experimental Free M3	Experimental M3 bound to *Pa*Man26A	Experimental M3 bound to *Pa*Man5A	Calculated Min I Φ= 42. Ψ= 5	Calculated Min II Φ= 23 Ψ= - 51
C1-B4	2.3	2.4	2.4	2.3	2.4
C1-B5	nd	3.8	nd	3.9	4.5
C1-B6	nd	2.9	3.1	2.5	4.2
C2-B4*	nd	nd	nd	4.3	3.7
C2-B6'*	nd	2.7	2.5	2.9	3.6
C5-B4	nd	3.9	nd	3.9	4.7

enzyme. It suggests that the energetic minimum I was more populated in both the bound states (Figure 2-3, Table 1). Thus, a conformer selection was revealed when **M3** bound to *Pa*Man26A and *Pa*Man5A mannanases.
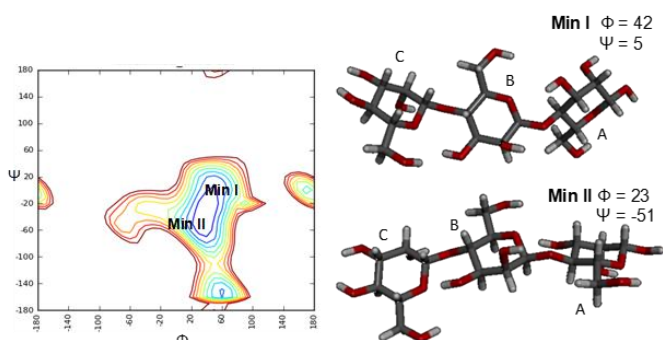
Figure 3: Adiabatic energy map of β- (1-4)-manno-oligosaccharide indicating the two global minima: one conformational state characterized from positive values of the inter-gycosidic dihedral angles (Min I), and one with positive Φ value and negative ψ value (Min II).

Binding epitope of the hydrolysis substrates to catalytic inactive mutants *Pa*Man26A-E390A and *Pa*Man5A-E283A

Two longer *manno*-oligosaccharide substrates, **M5** and **M6**, were then investigated in their interaction with catalytically inactive mutants of *Pa*Man26A and *Pa*Man5A. The replacement of the glutamate acting as nucleophile with an alanine residue (E390 and E283 for *Pa*Man26A and *Pa*Man5A respectively) impaired the catalytic activity of the enzymes. This impeded the oligosaccharide hydrolysis allowing us to investigate the whole substrates when bound to the proteins, in the absence of the hydrolysis products.
The comparison of STD NMR spectra showed that both substrates, the mannopentose and the mannohexose, were similarly

accommodated in the protein binding pocket (Figure 4-5, see also supporting information Table S3-S4). Although the severe overlap between proton signals, especially for those belonging to different internal **B** residues, hindered an accurate quantitative analysis, a qualitative estimation of STD enhancements permitted to identify the ligand moieties more involved in the interaction with each enzyme. As for the interaction with *Pa*Man26A-E390A (Figure 4) NMR data suggested that the entire oligosaccharides were in contact with the surface of the enzyme. As for the hydrolysis product recognition, the highest transfer of magnetization was observed for the proton at position 2 of the internal mannose residues, **B**; however, the presence of slighter STD signals belonging to the residues **C** and **A** indicated that also these moieties contributed to the binding.

In the case of the interaction of *Pa*Man5A-E283A with hydrolysis substrates (Figure 5), lower STD intensities were observed, once again suggesting that this enzyme bound more weakly to *manno*-oligosaccharides respect to the glycosidase *Pa*Man26A. However, the analysis of NMR data showed that **M5** and **M6** bound to the enzyme through a common manner, specifically via the non-reducing end of the molecule. In detail, H2 and H6 protons of terminal residue **C** exhibited high STD enhancements. The STD profile showed that also the residues **A** and **B** were involved in the interaction to some extent.

To resume, a comparison of the STD relative intensities belonging to the penta- and hexa-saccharidic substrates bound to mutant variants of *Pa*Man26A and *Pa*Man5A suggested a different mode of action of the two enzymes, supporting the hypothesis that the predominant binding mode was mediated by different protein subsites.
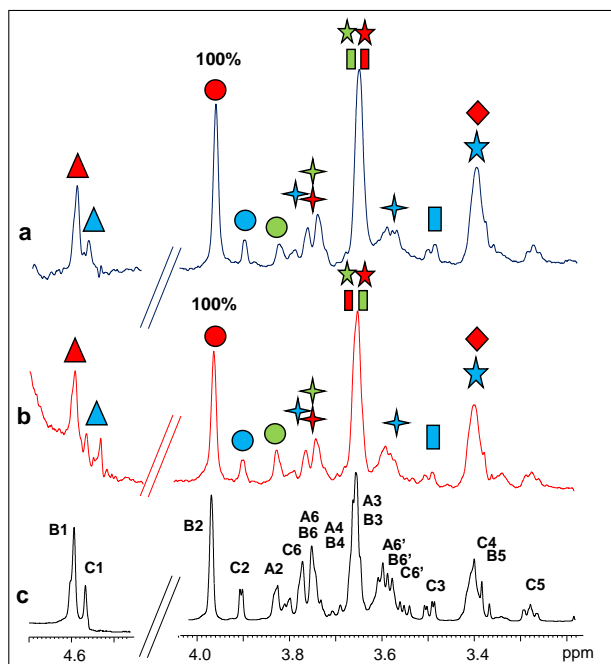
Figure 4. Binding of Pa*Man*26A-E390A to **M5** and **M6**. a) STD NMR spectrum on the mixture ***Pa*Man26A-E390A: M6.** b) STD NMR spectrum on the mixture ***Pa*Man26A-E390A: M5.** c) ^{1}H NMR spectrum of the mannohexose in the presence of the enzyme. The protein: ligand ratio was 1:50; the saturation time was set at 2 sec. The experimental temperature was 280K and the on resonance was set to 7.1 ppm. The numbers on the STD spectrum show the normalized levels of saturation (%) received by each ligand proton upon binding with the enzyme.
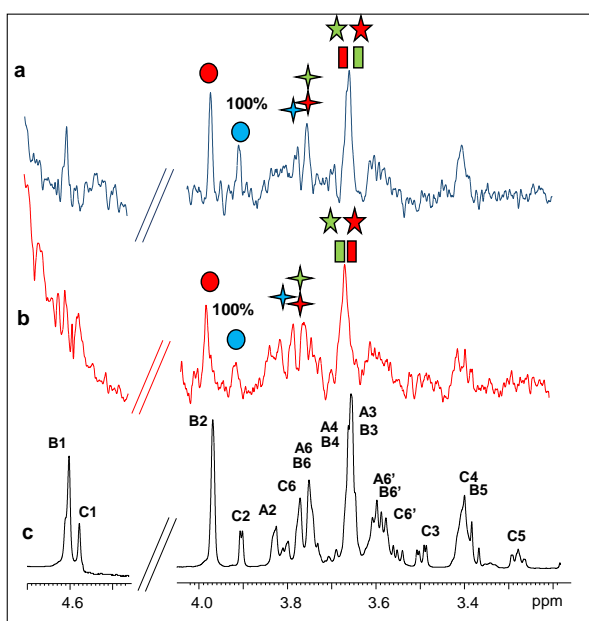
Figure 5. Binding of Pa*Man*5A-E283A to **M5** and **M6**. a) STD NMR spectrum on the mixture ***Pa*Man5A-E283A: M6.** b) STD NMR spectrum on the mixture ***Pa*Man5A-E283A: M5.** c) ^{1}H NMR spectrum of the mannohexose in the presence of the enzyme. The protein: ligand ratio was 1:50; the saturation time was set at 2 sec. The experimental temperature was 280K and the on resonance was set to 7.1 ppm.

Binding epitope of M5 to wild-type *Pa*Man26A and *Pa*Man5A

To further examine the mechanism of action of the *P. anserina* mannanases, we choose to investigate the interaction between the wild type enzymes, *Pa*Man26A and *Pa*Man5A, with the hydrolysis substrate **M5**. By using NMR spectroscopic techniques, we qualitatively estimated the contribution of the ligand moieties to the binding (Figure 6). The analysis of STD NMR effects (see also supporting information, Figure S1) confirmed previous results revealing striking differences between the *P. anserina* glycosidases mode of action. The pattern of STD enhancements of **M5** ligand when bound to *Pa*Man26A and *Pa*Man5A was indeed different, indicating the involvement to a major extent of different oligosaccharide moieties. In detail, although the whole oligosaccharide was accommodated in both proteins binding pocket, the recognition of the mannan substrates occurred mainly through the non reducing end of the ligand when bound to *Pa*Man5A. On the other hand, in the presence of the mannanase *Pa*Man26A, the internal mannose residues were more involved in the interaction with the enzyme.

All the above NMR data allowed to manually dock the mannopentose onto the 3D structure of both enzymes: *Pa*Man26A (PDB accession code 3ZM8, Figure 7) and *Pa*Man5A (PDB accession code 3ZIZ, Figure 8). The resulting complexes showed differences between the mannanases subsites involved in substrate binding (Figures 7-8).

Our STD NMR data were in agreement with the supposed presence of an added negative enzyme subsite (-4; nomenclature according to Davies et al.[15]) in the case of *Pa*Man26A. The protein aromatic residues Trp-244 and Trp-245, belonging to -4 subsite, indeed, made contacts with the terminal sugar of **M5**. These interactions contribute to stabilize the mannopentose in the -4 +1 subsites (Figure 7) promoting the uncommon cleavage of the reducing end of **M5.** This supported the hypothesis of an unusual arrangement of the oligosaccharide in the active site, as previously described. [12] The hydrolysis pattern derived from the cleavage of **M5** by *Pa*Man26A was indeed interestingly different from other GH26 endo-mannanases, including *Cj*Man26A from *C. japonicus*,[16] *BC*Man from *B. subtilis*,[17] and *Cf*MAn26A from *C. fimi*.[18]

On the contrary, *Pa*Man5A showed the usual pattern of hydrolysis with the release of **M3** and **M2** from **M5**, as explained by the lack of the negative protein subsite -4, which fosters a displacement of the substrate in the catalytic site with the consequent release of different hydrolysis products (Figure 8).

According to our study, indeed, the residue **C** is bound to the subsite -4 in *Pa*Man26A and in subsite -3 in *Pa*Man5A. It means that using **M3** as a substrate we have a unproductive binding (no product released). However, using **M5** as substrate we release M3 + M2 in the case of Man5A and M4 + M1 in the case of Man26A (which is unusual in endo-beta 1,4 mannanases). The latter is due to the fact that binding at the -4 subsite is strong, therefore the **M5** substrate spans form -4 to +1 subsites. Again, in *Pa*Man5A there is no -4 subsite so we cannot compare *Pa*Man26A and *Pa*Man5A regarding the -4 subsite.

Please do not adjust margins

Journal Name

ARTICLE

PaMan26A : M5

A

PaMan5A : M5

B

100%	> 50%
30-40%	< 30%
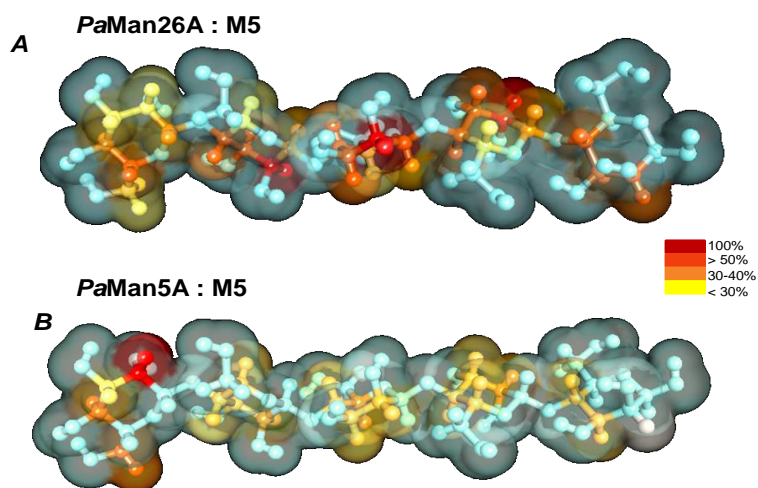
Figure 6. STD-derived epitope mapping on the molecular envelope of **M5** when bound to *Pa*Man26A (A) and *Pa*Man5A (B), with color coding from the highest (red) to lowest (yellow) observed STD effect according to the scale shown in the figure.

cleavage site

-4   -3   -2   -1   +1

M5 → M4 + M1

cleavage site

-3   -2   -1   +1   +2

M5 → M3 + M2
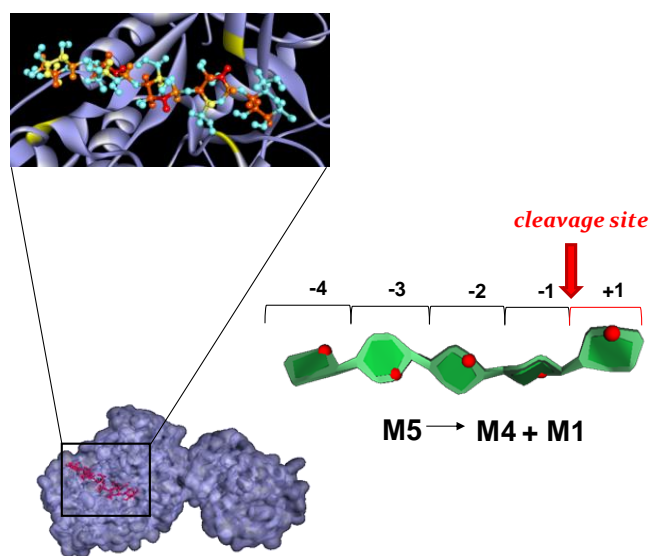
Figure 7. Mannopentose modelled into the proposed binding site of *Pa*Man26A (-4 +1 subsites).The PDB accession code for the structure *Pa*Man26A was under the number 3ZIZ. The glutamate residues of the active site involved in the interaction, as well as the Trp residues within the -4 subsite, were highlighted (yellow). The model of the bound ligand is consistent with NMR experimental data although it represented only one of disparate possible structures. The STD effects derived from a qualitative analysis of NMR spectra were reported on the molecular envelope of **M5** with color coding to the lowest (yellow) to the highest (red).The favorite cleavage site and main products for the **M5** hydrolysis when bound to *Pa*Man26A was depicted in stylized images on the right of the figures. The oligosaccharide structures were drawn by using the program Sweet Unity Mol (http://sourceforge.net/projects/unitymol/files/).
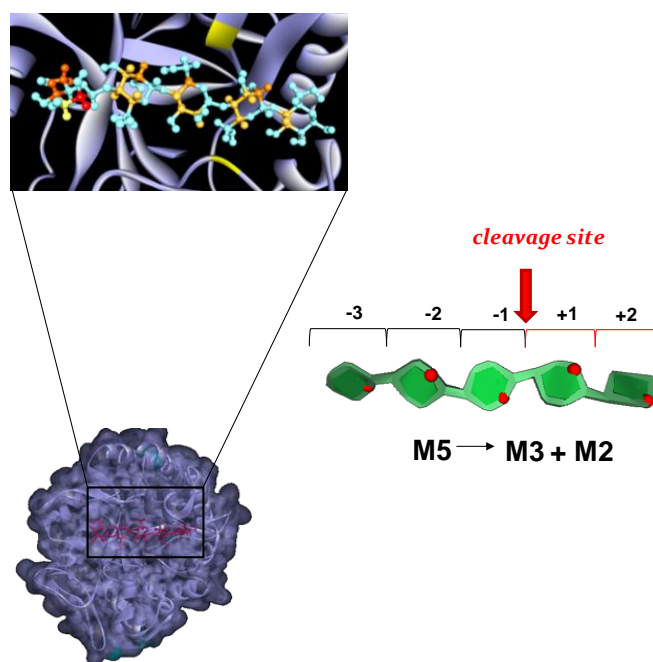
Figure 8. Mannopentose modelled into the proposed binding site of *Pa*Man5A (-3 +2 subsites). The PDB accession code for the structure *Pa*Man5A was under the number 3ZM8. The glutamate residues of the active site involved in the interaction were highlighted (yellow). The model of the bound ligand is consistent with NMR experimental data although it represented only one of disparate possible structures. The STD effects derived from a qualitative analysis of NMR spectra were reported on the molecular envelope of M5 with color coding to the lowest (yellow) to the highest (red).The favorite cleavage site and main products for the M5 hydrolysis in the presence of *Pa*Man5A was depicted in stylized images on the right of the figures. The oligosaccharide structures were drawn by using the program Sweet Unity Mol (http://sourceforge.net/projects/unitymol/files/).

Experimental

PaMan26A and PaMan5A wild-type and mutant production and purification. *Pa*Man26A and *Pa*Man5A were produced in *Pichia pastoris* as previously described,[19,20] and *Pa*Man26A-E390A and *Pa*Man5A-E283A were also produced in *P. pastoris* as described in Couturier et al, 2013. Purification was carried out as described in Couturier et al, 2013. Briefly, the first step of purification consisted in an affinity chromatography using a nickel chelate His-Bind Resin (GE Healthcare) equilibrated with 50 mM Tris-HCl (pH 7.8), 150 mM NaCl, and 10 mM imidazole. The concentrated *P. Pastoris* supernatant was diluted into the equilibration buffer and loaded onto the column at 4°C. The enzyme was eluted with the same buffer containing 150 mM imidazole. Further purification was achieved by an additional size exclusion chromatographic step. The eluate was concentrated using a Vivaspin with 10-kDa cut-off polyethersulfone membrane, (Sartorius, Palaiseau, France) and dialysed in Hepes 20 mM pH 7.5, NaCl 150 mM. The concentrated fraction was subsequently loaded onto a Superdex S200 HiLoad 16/60 column (Amersham, Buckinghamshire,UK). The fractions containing the enzyme were pooled and concentrated using a Vivaspin with 10 kDa cut-off polyethersulfone membrane.

NMR spectroscopy. All the experiments were recorded on a Bruker 600 MHz DRX spectrometer equipped with a cryo probe at 280K. The samples were dissolved in deuterated phosphate buffer (PBS) at pH 6.5, and spectra were calibrated by using [D4] (trimethylsislyl)propionic acid sodium salt (TSP, 10mM) as internal reference. The enzymes were exchange in PBS by vivaspin filters and a protein concentration of 20uM (in 500ul) was used for all the experiments.

All the ligands (prepared by controlled enzymic hydrolysis of mannan) were purchased from Megazyme International (Bray, Ireland).

The ligands proton resonances were assigned by employing a combination of 1D and 2D NMR experiments including COSY, TOCSY, NOESY and HSQC (see supporting information). ^{1}H NMR spectra were acquired with 32 k and 64 k data points. Double quantum-filtered phase sensitive COSY experiments were performed by using data sets of 4096 x 512 (t1 x t2) points. Total Correlation Spectroscopy (TOCSY) spectra were acquired with a with a spin lock time of 100 ms and data sets of 4096 x 256 points. Nuclear Overhauser enhancement spectroscopy (NOESY) spectra were measured with data sets of 4096 x 256 points; mixing times between 100 and 600 ms were used. Heteronuclear single quantum coherence (HSQC) experiments were measured in the [1]H-detected mode via single quantum coherence with proton decoupling in the ^{13}C domain, by using data sets of 2048 x 256 points. Experiments were carried out in the phase-sensitive mode according to the method of States at al.[21] In all homonuclear spectra the data matrix was zero-filled in the F1 dimension to give a matrix of 4096 x 2048 points and resolution was enhanced in both dimensions by a cosine-bell function before Fourier transformation

For the bound ligands, STD NMR experiments were carried out with 672 scans and 32 dummy scans. The pseudo 2D pulse programs stddiff, stddiff.3 and stddiffesgp.3 were used; the broad signals of the proteins were eliminated by using a T_{1p} filter of 50ms. The protein –ligand ratio varied from 1:50 to 1:100, with a protein concentration of 20 μM in 500 μl, and a saturation of 2 sec was

used. The protein was saturated employing a train of 40 Gauss pulse with a length of 50 ms. The on-resonance frequency was set at δ= 0.4 or 7 ppm (regions in which no ligand resonances were observed), whereas the off resonance pulse frequency was set at 40 ppm. The original FID were zero filled up to 64k data and processed with the use of exponential window function in order to increase the S/N ratio. The 2D STD –HSQC were carried out by using a data set of 2048 x 256 points; the same parameters used for STD and HSQC spectra were used.

The STD effect was calculated by $(I_0 - I_{sat})/I_0$, where $(I_0 - I_{sat})$ is the intensity of the signal in the STD NMR spectrum and I0 is the peak intensity of an unsaturated reference spectrum (off-resonance). The highest STD enhancement was set to 100% and the other signals were normalized to this peak. Tr-NOESY experiments were recorded by using a protein-ligand molar ratio 1:20 with mixing times varying between 100 and 600 ms. Data acquisition and processing were performed with TOPSPIN software.

Conformational analysis. The MM3* force field as included in MacroModel 8.0 was used to perform molecular mechanics calculation with a dielectric constant of 80. The dihedral angles were varied incrementally using a grid step of 18°. The molecular dynamic simulations were run by using the MM3* force field; bulk water solvation was simulated by using MacroModel generalized Born GB/SA continuum solvent model. Simulations were performed at 300 K, structures were initially subjected to an equilibration time of 300 ps, then a 5000 ps molecular dynamic simulation was performed with a dynamic time-step of 1.5 fs, a bath constant t of 0.2 ps and the SHAKE protocol to the hydrogen bonds. Ensemble average-interproton distances were calculated using the NOEPROM program. Surfaces were calculated with the Surface utility of Macromodel and with Molecular Surface displays of ViewerPro Version 4.2.

Docking of the NMR derived mannopentose structure to the *Pa*Man26A and *Pa*Man5A (PDB 3ZM8 and 3ZIZ respectively) was performed manually using using the PyMOL Molecular Graphics System (Version 1.Or1, Schrçdinger, LLC).

Conclusions

The comprehension of the complex lignocellulolytic enzymatic machineries of bacteria and fungi is attracting an increasing attention in the frame of renewable biofuel production through the saccharification of plant cell walls. The coprophilic fungus *Podospora anserina* possesses one of the largest set of enzymes ascribed to the deconstruction of biomass and candidate for the production of environmental friendly organic fuel. Therefore, the knowledge at atomic resolution of plant cell wall polysaccharide recognition by *P. anserina* glycoside hydrolases resides at the basis of the potential development of novel biocatalysts essential for applications in industrial and biotechnological fields.

In the present study, we have focused on two *P. anserina* glycosidases with affinity for hemicellulosic polysaccharides. In detail, the outcomes of our work have provided in depth structural features on the molecular recognition of plant cell wall oligomannosides by two *P. anserina* β-mannanases, *Pa*Man26A and *Pa*Man5A. The bioactive conformations and the epitope mapping of *manno*-oligosaccharides bound to both enzymes were revealed by

ARTICLE

means of advanced, ligand-based NMR spectroscopic techniques. Such biophysical methods have been already used to characterize members of glycoside hydrolase families included in the database of CAZymes,[22] providing exclusive information on the receptor-ligand binding mechanisms, difficult to achieve with other methods. Here, STD NMR and tr-NOE experiments permitted to draw an accurate picture of mannans binding in solution, shedding light on the conformation and the topography of different oligosaccharides bound to the *P. anserina* β-mannanases. The comparison between the STD NMR profiles of the two different glycosidases, *Pa*Man26A and *Pa*Man5A, when bound to the same ligand, clearly showed that they displayed a different mode of *manno*-oligosaccharides recognition. Indeed, although both mannanases accommodated the whole oligosaccharide backbone in the binding pocket, the interaction with the glycoside hydrolase *Pa*Man26A involved the internal residues of mannose in a major extent. On the other side, the *Pa*Man5A preferentially recognized the terminal end of *manno*-oligosaccharides. Furthermore, NMR data showed that the mode of action of each glycosidase remained the same in the presence of both enzyme substrates and the hydrolysis products.

Thus, an accurate NMR analysis permitted to demonstrate that, in contrast with other glycoside hydrolases belonging to the GH26 family, [16,17,18] *Pa*Man26A exhibited an unusual arrangement of *manno*-oligosaccharides in the binding pocket, due to the presence of a peculiar negative -4 protein subsite. On the contrary, *Pa*Man5A showed the classical mannan hydrolysis pattern. According to the published GHs X-ray structures, the recognition and binding of plant cell wall *manno*-oligosaccharides involved different enzyme subsites between the two families of glycoside hydrolases GH26 and GH5. Notably, our findings are in agreement with the existing hypothesis,[12] and further suggest a different arrangement of the proteins binding pocket, with the active site of *Pa*Man26A consisting of up to four negative and two positive enzyme subsites (-4 +2). On the contrary, *Pa*Man5A exhibited three positive and three negative enzyme subsites (-3 +3) with a consequent different specificity, mode of action and likely biological role between the two enzymes.

The reported data represent a good starting point to significantly enhance the activity of the fungal endo-mannanases through a molecular engineering approach.[22] Therefore, our comparative analysis shed more light on the *P. anserina* enzymatic machinery and it may help to improve the use of biocatalysts in industrial applications.

Acknowledgements

Notes and references

1   a) M.A. O'Neill, W.S. York, *The plant cell wall,* 2003,1-54; b) J: Vogel, *Current opinion in plant biology,* 2008, **11**(3), 301-307.

2   K.S. Mikkonen, M. Tenkanen, *Trends in Food Science & Technology,* 2012, **28**(2), 90-102.

3   A.H. Liepman, C.J. Nairn, W.G.T. Willats, I. Sørensen, A.W. Roberts, K. Keegstra, *Plant Physiology,* 2007, **143**, 1881–1893.

4   a) L.E. Tailford, V.M. Ducros, J.E. Flint, S.M. Roberts, C. Morland, D.L. Zechel, N. Smith, M.E. Bjornvad, T.V. Borchert, K.S. Wilson *et al*, *Biochemistry,* 2009, **48**(29), 7009-7018; b) W.H. Van Zyl, S.H. Rose, K. Trollope, J.F. Görgens, *Process Biochemistry,* 2010, **45**(8), 1203-1213.

5   a) B. Henrissat, *Biochemical Journal* 1991, 280, 309–316; b) B. Henrissat, A. Bairoch, *Biochemical Journal Letters,* 1996, **316**, 695–696.c) V. Lombard, H. Golaconda Ramulu, E. Drula, PM Coutinho, B Henrissat, *Nucleic Acids Res,* 2014, **42**, D490–D495.

6   a) A. Helenius, M. Aebi, *Science,* 2001, **291**, 2364–2369; b) H. Kitagaki, K. Ito, H. Shimoi, *Eukaryotic Cell,* 2004, **3**, 1297–1306; c) B. Henrissat, I. Callebaut, S. Fabrega, P. Lehn, J. P. Mornon, G. Davies, *Proc. Natl. Acad. Sci. USA,* 1995, **92**, 7090 – 7094.

7   P. Tiwari, B.N. Misra, N.S. Sangwan *Biomed Res Int.,* 2013, 203735.doi: 10.1155/2013/203735.

8   L. Thomas, A. Joseph, L.D. Gottumukkala, *Bioresour Technol*., 2014, **158**, 343-50.

9   a) D. Hogg, E.J. Woo, D.N. Bolam, VA. McKie, HJ. Gilbert, RW. Pickersgill, *J Biol Chem.,* 2001, **276**(33),31186-92; b) L.E. Tailford, V.M. Ducros, J.E. Flint, S.M. Roberts, C. Morland, D.L. Zechel, N. Smith, M.E. Bjørnvad, T.V. Borchert, K.S. Wilson, G.J. Davies, H J. Gilbert, *Biochemistry,* 2009, **48**, 7009–7018; c) H. Tsukagoshi, A. Nakamura, T. Ishida, K.K. Touhara, M. Otagiri, S. Moriya, M. Samejima, K. Igarashi, S. Fushinobu, K. Kitamoto, M. Arioka, *J.Biol.Chem.* 2014, **289**, 10843-10852. d) Y. Zhao, Y. Zhang, Y. Cao, J. Qi, L Mao, et al., *PLoS ONE,* 2011, 6(1), e14608; e) M.K. Kim, Y.J. An, J.M. Song, C.S. Jeong, M.H. Kang, K.K. Kwon, Y.H. Lee, S.S. Cha, *Proteins,* 2014, **82**(11),3217-23.

10 a) E. Sabini, H. Schubert, G. Murshudov, K.S. Wilson, M. Siika-Aho, M. Penttilä, *Acta Crystallogr. D. Biol. Crystallogr.,* 2000, **56**, 3–13; b) R. Bourgault, A.J. Oakley, J.D. Bewley, M.C. Wilce, *Protein Sci*. 2005, **14**, 1233–1241; c) A.M. Larsson, L. Anderson, B. Xu, I. G. Muñoz, I. Usón, J.C. Janson, H. Stålbrand, J. Ståhlberg, *J. Mol. Biol.,* 2006, **357**, 1500–1510.

11 D.N. Bolam, N. Hughes, R. Virden, J.H. Lakey, G.P. Hazlewood, B. Henrissat, H.J. Gilbert, *Biochemistry,* 1996, **35,** 16195–16204.

12 M. Couturier, A. Roussel, A. Rosengren, P. Leone, H. Stålbrand, J-G Berrin, *J Biol Chem,* 2014, **289**, 31088-31101.

13 R. Marchetti, A. Molinaro, A. Silipo, "NMR as a Tool to Unveil the Molecular Basis of Glycan-mediated Host–Pathogen Interactions" RSC Drug Discovery Series No. 43; *Carbohydrates in Drug Design and Discovery* (Eds: J. Jimenez-Barbero, J. F. Canada and S. Martın-Santamarıa), 2015, pp-21-37.

14 A. Poveda, J.L. Asensio, J.F. Espinosa, M. Martin-Pastor, J. Cañada, J. Jiménez-Barbero *J Mol Graph Model.,* 1997, **15**(1),9-17, 53.

15 G.J. Davies, K.S. Wilson, B. Henrissat, *Biochem. J.,* 1997, **321**, 557 –559.

16 V.M. Ducros, D.L. Zechel, G.N. Murshudov, H.J. Gilbert, L. Szabó, D. Stoll, S.G. Withers, G.J. Davies, *Angew Chem Int Ed Engl.,* 2002, **2**;41(15),2824-7.

17 Y. Xiao-Xue, A. Xiao-Min, G. Lu-Lu, L. Dong-Cai, *Journal of Molecular Biology,* 2008, **379**, 535-544.

18 J. Le Nours, L. Anderson, D. Stoll, H. Stålbrand, L. Lo Leggio. *Biochemistry,* 2005, **44**, 12700-12708.

19 M. Couturier, J. Féliu, S. Bozonnet, A. Roussel, J-G Berrin, *PLoS One,* 2013, **22**, 8(11),e79800.

20 M. Couturier, M. Haon, P.M. Coutinho, B. Henrissat, L. Lesage-Meessen, J-G Berrin, *AEM,* 2011, **77**(1),237-46.

21 D. J. States, R. A. Haberkorn, D.J. Ruben, *Magn. Reson.,* 1882, **48**, 286-292.
22 A. Silipo, J. Larsbrink, R. Marchetti, R. Lanzetta, H. Brumer, A. Molinaro. *Chemistry*, 2012, **18**(42), 13395-404.